Chem

CellPress

Article

# A Structural Mimic of Carbonic Anhydrase in a Metal-Organic Framework

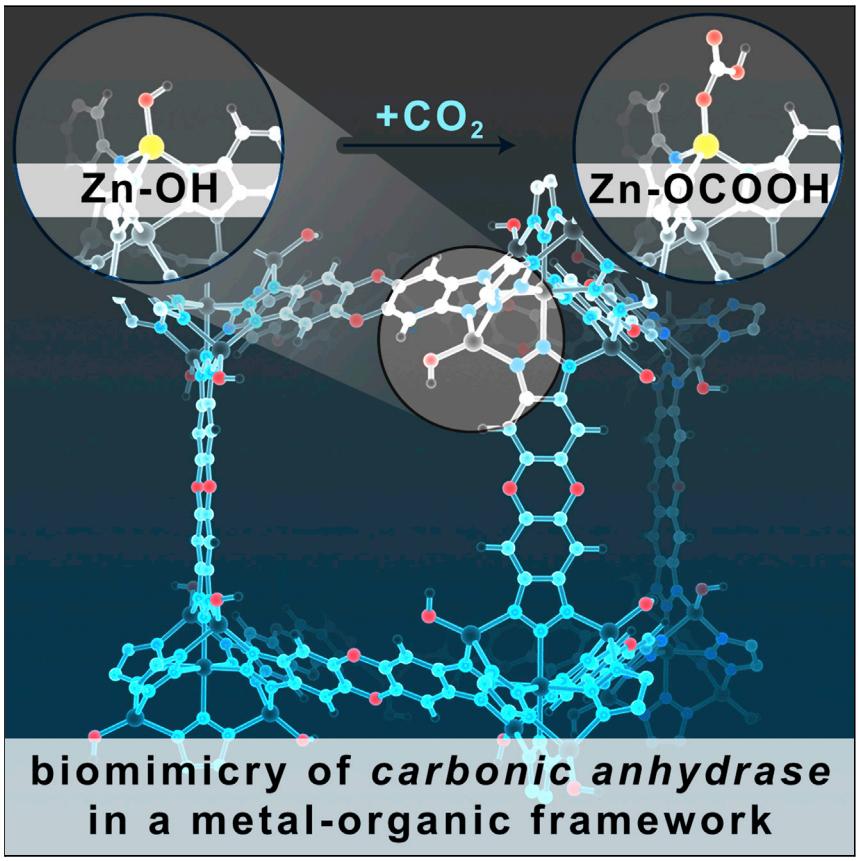


The nodes of metal-organic frameworks are attractive sites for mimicking metalloenzymes, primarily through their site isolation and similar ligand fields. In this article, the metal-organic framework MFU-4l is shown to mimic the active site of carbonic anhydrase with high structural fidelity and reactivity. The material adsorbs high quantities of carbon dioxide at low pressures and mimics critical features of carbonic anhydrase, such as isotopic exchange of oxygen atoms from water and carbon dioxide.

Ashley M. Wright, Zhenwei Wu, Guanghui Zhang, ..., Christopher H. Hendon, Jeffrey T. Miller, Mircea Dincă

mdinca@mit.edu

## HIGHLIGHTS

Hydroxylation of the MFU-4*l* metal node creates a functioning carbonic anhydrase mimic

High uptake volumes of adsorbed carbon dioxide occur at low pressures

Isotopic exchange of $^{18}O$ from $H_2O$ into $CO_2$ is catalyzed by MFU-4*l*-(OH)

Wright et al., Chem 4, 2894–2901
December 13, 2018 © 2018 Elsevier Inc.
https://doi.org/10.1016/j.chempr.2018.09.011

Chem

CellPress

Article

# A Structural Mimic of Carbonic Anhydrase in a Metal-Organic Framework

Ashley M. Wright,[1] Zhenwei Wu,[2] Guanghui Zhang,[2] Jenna L. Mancuso,[3] Robert J. Comito,[1] Robert W. Day,[1] Christopher H. Hendon,[3] Jeffrey T. Miller,[2] and Mircea Dincă[1,4,*]

## SUMMARY

**Metal-organic frameworks (MOFs) have exciting potential for biomimetic studies of enzymes, yet construction of high-fidelity models at the metal nodes is challenging. Nonetheless, biomimetic MOFs have significant advantages, such as increased stability and ease of separation, over their enzymatic and homogeneous counterparts, making them particularly attractive for industrial applications. Here, we demonstrate biomimetic behavior of Zn hydroxide moieties inside a MOF with structural and reactivity characteristics of carbonic anhydrase. Similar to the biological system, the MOF binds $CO_2$ by an insertion mechanism into the Zn–OH bond, leading to significant adsorption of $CO_2$ (3.41 mmol/g). In reactivity mimicking that of the enzyme, the material also catalyzes the oxygen isotope exchange between water and carbon dioxide. Overall, these results provide the strongest evidence yet of metal nodes in MOFs bearing high structural fidelity to enzymatic active sites.**

## INTRODUCTION

Metal-organic frameworks (MOFs) are promising platforms for biomimetic studies of metalloenzymes.[1–4] The connecting ends of organic linkers in MOFs, such as carboxylates and triazoles, are comparable to the ligands that make up the active sites in metalloenzymes. Consequently, the metal nodes are attractive targets for biomimetic chemistry. The advantages of performing biomimetic chemistry in MOFs over traditional homogeneous systems include (1) site isolation, preventing unwanted bimetallic reactivity and in turn allowing for sterically unhindered metal sites;[5] (2) tunable pore environments, affording hydrophilic or hydrophobic channels, which can mimic the channels found in the enzymes;[3] and (3) higher stability than with enzymes,[6–9] potentially leading to broader use of biomimetic chemistry in industrially relevant applications.

Carbonic anhydrase (CA) is a ubiquitous zinc metalloenzyme that catalyzes the hydration of carbon dioxide. The active site of CA features a divalent zinc in a $N_3ZnOH$ coordination environment, where the zinc exhibits a tetrahedral geometry featuring three histidine groups and a hydroxide (or water) (Figure 1).[10] Much has been learned about CA through modeling the active site with synthetic analogs,[11] such as $Tp^{(tBu,Me)}ZnOH$ (Tp = tris(pyrazolyl)hydroborate), which reacts reversibly with $CO_2$ and catalyzes oxygen atom exchange between $CO_2$ and $H_2O$.[12–14] Accessing similar Tp-like environments within MOFs would afford site-isolated examples of CA. One material whose secondary building units (SBUs) are almost exact structural mimics of the active site in CA is MFU-4l ($Zn_5Cl_4(BTDD)_3$ **1**, where $BTDD^{2-}$ = bis(1,2,3-triazolo[4,5-*b*],[4′,5′-*i*])dibenzo[1,4]dioxin) (Figure 1).[15–20] The SBUs, or metal nodes, in this material feature four peripheral zinc chloride sites that are coordinated by three triazoles in $C_3$ symmetry analogous to the Tp ligand and, accordingly, CA (Figure 1).

### The Bigger Picture

Mimicking metalloenzymes at the node of a metal-organic framework (MOF) has the potential to impart enzyme-like catalytic activity within a heterogeneous material. Carbonic anhydrase, one of nature's fastest enzymes, catalyzes the hydrolysis of carbon dioxide into bicarbonate and protons. Notably, carbonic anhydrase mimics have been proposed as potential catalysts for carbon capture and sequestration from the environment. Here, we demonstrate that the metal node of MFU-4*l*, a MOF featuring a metal node with a $N_3ZnX$ coordination environment, can be functionalized to give a mimic of carbonic anhydrase. This work describes a well-defined example of a metal node within a MOF with high structural fidelity to an enzyme active site. It has potential applicability to applications such as $CO_2$ capture and sequestration and also important gas separations involving $CO_2$.

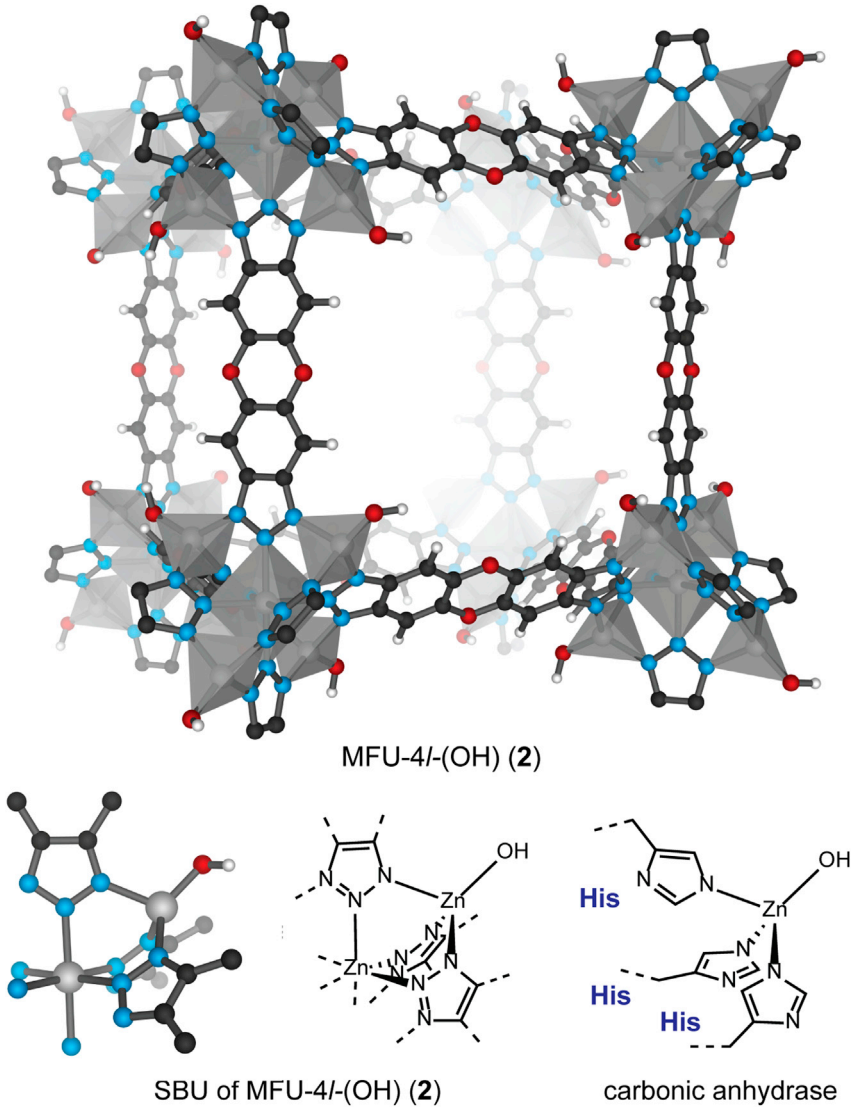


**Figure 1. Structure of MFU-4*l*-(OH) (Top) and Comparison of the Active Site in Carbonic Anhydrase with the Peripheral Zinc in MFU-4*l* (Bottom)**

The structure of MFU-4l-(OH) (**2**) was modeled from the XYZ coordinates of an extended lattice DFT model.

In this article, we demonstrate that the metal node of MFU-4*l* (**1**) can be modified by anion exchange to create a biomimetic model of CA. The addition of organic hydroxide affords MFU-4*l*-(OH) (**2**), where original terminal $N_3Zn$–Cl centers are quantitatively transformed to terminal $N_3Zn$–OH units. Characterization by X-ray absorption spectroscopy confirms the installation of the hydroxide unit, and subsequent reactivity studies show that **2** reacts with $CO_2$ and catalyzes oxygen atom exchange between $H_2O$ and $CO_2$ as well as the hydrolysis of 4-nitrophenyl acetate (4-NPA), consistent with the activity of CA.

## RESULTS AND DISCUSSION

Although the terminal chlorides in MFU-4*l* are known to exchange with a variety of other anions, hydroxide exchange using KOH has been reported to cause decomposition.[21] However, we found that anion metathesis with hydroxide was

[1]Department of Chemistry, Massachusetts Institute of Technology, 77 Massachusetts Avenue, Cambridge, MA 02139, USA

[2]Davidson School of Chemical Engineering, Purdue University, 480 Stadium Mall Drive, West Lafayette, IN 47907, USA

[3]Materials Science Institute, Department of Chemistry and Biochemistry, University of Oregon, Eugene, OR 97403, USA

[4]Lead Contact

*Correspondence: mdinca@mit.edu

https://doi.org/10.1016/j.chempr.2018.09.011

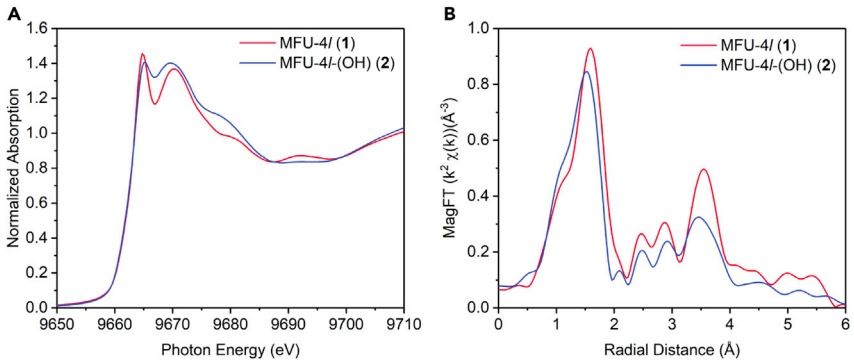


**Figure 2. X-Ray Absorption Plots of MFU-4*l* (1) and MFU-4*l*-(OH) (2)**

(A) XAS plot of the zinc K-edge XANES spectra for MFU-4*l* (**1**, red trace) and MFU-4*l*-(OH) (**2**, blue trace).

(B) Magnitude of Fourier transform of $k^2$-weighted EXAFS spectra of MFU-4*l* (**1**, red trace) versus MFU-4*l*-(OH) (**2**, blue trace).

possible through the addition of 10 equiv (2.5 equiv per peripheral zinc) of tetrabutylammonium hydroxide, [TBA][OH], to a suspension of **1** in methanol, which yielded MFU-4*l*-(OH) ($Zn_5(OH)_4(BTDD)_3$, **2**) as a beige microcrystalline solid. Analysis of **2** by powder X-ray diffraction confirmed the retention of crystallinity (Figure S1). Fitting a 77 K $N_2$ adsorption isotherm of **2** to the Brunauer-Emmett-Teller equation gave a surface area of 2,739 $m^2/g$, which, although lower than that of **1** (3,525 $m^2/g$), confirmed the retention of porosity after treatment with base (Figure S2). Thermogravimetric analysis of **2** revealed that it is less stable than its parent **1**; its extrapolated onset decomposition temperature occurs at 250°C, approximately 100°C lower than for **1** (Figure S6). Energy-dispersive X-ray spectroscopy and X-ray photoelectron spectroscopy of **2** confirmed the quantitative replacement of chloride with hydroxide and revealed no chlorine-specific peaks (Figures S4 and S5). Finally, diffuse reflectance infrared Fourier transform spectroscopy (DRIFTS) of **2** revealed a hydroxide O–H stretching band at 3,699 $cm^{-1}$, a signal that was not observed in the DRIFTS data for **1** (Figure S9). Indeed, the frequency of this band is comparable to that of the OH stretch found in the homologous molecular compound $Tp^{tBu,Me}Zn(OH)$ (3,676 $cm^{-1}$).[11,12]

To further characterize the incorporation of a Zn–OH site in **2**, we analyzed the material by X-ray absorption spectroscopy (XAS). Whereas both **1** and **2** had the same Zn K-edge energy (9,663.6 eV), indicating a common oxidation state on zinc in both materials (Figure 2A), a significant difference in the zinc coordination environment became apparent when we compared the white line and near-edge regions for the two materials: **2** exhibited a lower and broader white line than **1** and a near-edge feature (~9,668 eV) higher than that of **1** (Figure 2A). Moreover, the extended X-ray absorption fine structure (EXAFS) spectra of **1** and **2** indicated a difference in the primary coordination sphere of zinc. In **2**, the first shell peak shifted to a lower radial distance and was less intense than the corresponding peak in **1** (Figure 2B), consistent with a shorter Zn–X bond and scattering by a lighter element, such as oxygen. Quantitative fitting of the EXAFS region for **2** was challenging because there were two $Zn^{2+}$ sites ($N_3ZnX$ and $N_6Zn$) with distinct coordination environments, and the small difference between the Zn–N bond length of the two sites made it difficult to fit them as one path or separate paths. Consequently, we chose to fit the difference spectrum of **1** and **2**; the similar coordination environments of the two Zn sites removed the disordered Zn–N scattering in the data, and the fit provided information regarding the Zn–X bond (see Figures S7 and S8 for further details). As a result,

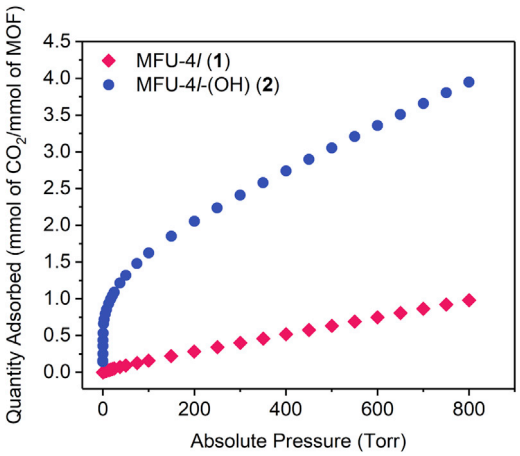


**Figure 3. $CO_2$ Isotherm at 298 K for MFU-4*l* (1; Red Diamonds) and MFU-4*l*-(OH) (2; Blue Circles)**

we obtained a satisfactory fit for the Zn–Cl bond distance of 2.17 Å in **1** and for the Zn–O bond distance of 1.93 Å in **2**. For comparison, an extended lattice calculation on **2** (**2**-DFT [density functional theory]) computed a Zn–O bond distance of 1.84 Å (see Supplemental Information), in good agreement with the EXAFS fitting (1.85 Å for comparable molecular analogs) and with CA itself (1.9–2.1 Å).[11]

A critical step in $CO_2$ hydration by CA is $CO_2$ insertion into the Zn–OH bond. After confirming the installation of the Zn–OH group, we probed its reactivity with $CO_2$ by measuring its $CO_2$ adsorption isotherm at 25°C (Figures 3 and S3). Notably, the adsorption isotherm profile featured a significant uptake of $CO_2$ between 0 and 17 Torr, corresponding to 0.86 mmol of $CO_2$ per g of MOF. Importantly, this is equivalent to 1.0 mmol of $CO_2$ per mmol of MOF or the insertion of $CO_2$ into one of four Zn–OH sites in each SBU. The isotherm profile became shallower, and uptake of the remaining ~75% $CO_2$ occurred over a large pressure range of 17–800 Torr. The total $CO_2$ adsorption capacity at 800 Torr was 3.41 mmol/g (4.05 mmol of $CO_2$ per mmol of MOF), which coincides with the total number of Zn–OH sites (3.36 mmol/g) in the MOF. The initial steep uptake supports a strong interaction between **2** and the first $CO_2$ equivalent (per SBU), most likely stemming from the insertion of $CO_2$ into the Zn–OH bond, a unique $CO_2$ capture mechanism that has been observed only once before in a MOF.[22] After the initial steep uptake, the isotherm profile became shallower with increasing coverage, suggesting a change in the interaction between the MOF and $CO_2$ or a shifting of the hydroxide-carbonate equilibrium with increasing $CO_2$ pressure.

To gain more insight into the framework-adsorbate interaction, we determined the coverage-dependent $CO_2$ adsorption enthalpy ($Q_{st}$) by measuring the $CO_2$ adsorption isotherms at three different temperatures (288, 298, and 308 K) and fitting the isotherm data to the virial equation (Figures S13 and S14).[23,24] Other fitting routines, including the Langmuir, Langmuir-Freundlich, and two-site Langmuir models, provided less satisfactory fits (Figures S11 and S12). With the virial equation, $Q_{st}$ at zero $CO_2$ coverage is 81 kJ/mol, a value much higher than those typically observed in MOFs and other microporous materials[25] and consistent with a chemisorption event. Indeed, the $Q_{st}$ for $CO_2$ insertion into metal–hydroxide bonds in $[Mn^{II}Mn^{III}(OH)Cl_2(bbta)]$ and $[Co^{II}Co^{III}(OH)Cl_2(bbta)]$ ($H_2bbta$ = 1*H*,5*H*-benzo(1,2-d:4,5-d)bistriazole) is 99 and 110 kJ/mol, respectively.[22] Notably, the coverage-dependent $Q_s$ suggests a bimodal adsorption profile (Figure S15). With increasing

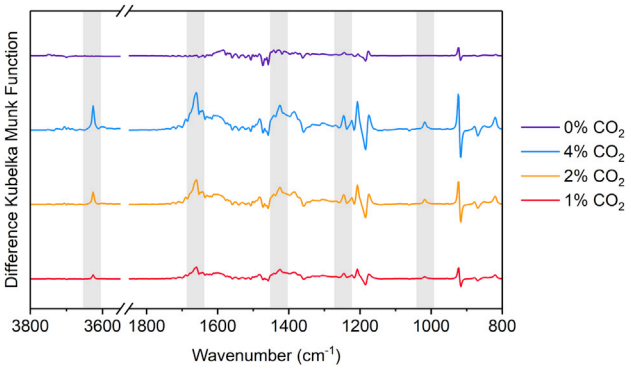


**Figure 4. Difference DRIFTS Plots Collected on MFU-4*l*-(OH) (2) with Increasing Concentrations of $CO_2$ in an Argon Carrier Gas**

The shaded areas denote new bands assigned to vibrations of a bicarbonate ligand ($HCO_3^-$). The purple trace (0% $CO_2$) was collected after the blue trace (4% $CO_2$).

coverage, $Q_{st}$ stays relatively constant up to ~0.5 equiv of $CO_2$ per SBU and then gradually decreases until it reaches ranges between 62 and 35 kJ/mol for the second $CO_2$ equivalent and between 35 and 20 kJ/mol for the third $CO_2$ equivalent. The large, bimodal variation in $Q_{st}$ suggests that the adsorption mechanism changes with increasing $CO_2$ coverage.

We modeled $CO_2$ insertion into the Zn–OH bond by using DFT (PBE/6-311G**). To do so, we used a truncated model of the SBU, $Zn_5(OH)_4(BTA)_6$ (BTA = benzotriazole). Optimization of the cluster model gave a Zn–O(H) bond distance of 1.85 Å and Zn–N bond distances of 2.02–2.05 Å, consistent with the EXAFS fit and extended lattice DFT model. Notably, although the calculated enthalpy of $CO_2$ insertion into the first Zn–OH unit was −50 kJ/mol, the second, third, and fourth $CO_2$ molecules were calculated to bind, also by insertion into Zn–OH units, with a lower energy of approximately −44 kJ/mol. The trend of decreasing binding enthalpy is also in qualitative agreement with the experimental data. We postulate that the conversion of the highly basic –OH to weakly basic $–OCO_2H$ perturbs the coordination environment of the SBU enough to weaken the nucleophilicity of the remaining three Zn–OH sites within a given metal node. Given that the nucleophilic strength of Zn–OH correlates with its reactivity toward $CO_2$,[26] less nucleophilic Zn–OH units shift the Zn–OH + $CO_2$ ⇌ $Zn–OCO_2H$ equilibrium to the left. A comparable trend of initially high heat of adsorption to lower heat of adsorption was observed in $[M^{II}M^{III}(OH)Cl_2(bbta)]$.[22]

To determine the nature of the chemisorption interaction, we monitored the reaction between **2** and $CO_2$ by DRIFTS. Exposing **2** to incremental increases in [$CO_2$] from 1,000 to 4,000 ppm in an argon carrier gas resulted in the formation of new bands in the DRIFT spectrum (Figure 4). By contrast, the addition of $CO_2$ to **1** under the same conditions resulted in no spectral changes (Figures S22 and S23). The new spectral features in **2** are consistent with the formation of a zinc bicarbonate, which is also the product of $CO_2$ insertion in CA. Specifically, a new band at 3,626 $cm^{-1}$ was assigned to the O–H stretch.[13] Bands at 1,660 and 1,245 $cm^{-1}$ corresponded to the O=C–O asymmetric and symmetric stretches, respectively.[13] Additionally, bands at 1,018 and 1,423 $cm^{-1}$ were associated with bending and stretching vibrations of the COH group in bicarbonate. The observed stretches were comparable to those of the molecular analog $^{tBu,Me}TpZn(OCO_2H)$, which featured asymmetric and symmetric O=C–O stretches at 1,675 and 1,302 $cm^{-1}$, respectively.[13] In addition, the IR

spectrum of [$Mn^{II}M^{III}(OCO_2H)Cl_2$(bbta)] (M = Mn, Co) featured stretches at 3,682 (O–H), 1,224 (symmetric O–C=O), and 1,050 $cm^{-1}$ (O–H bending).[22] Purging the DRIFTS setup with 100% argon flow resulted in the loss of the new signals and reformation of the starting spectrum, consistent with a reversible reaction with $CO_2$.

We further illustrated the critical role of the hydroxide ligand in $CO_2$ uptake by comparing the $CO_2$ sorption properties of **1** and **2**. MOF **1**, containing a Zn–Cl bond and a saturated metal center, showed a $CO_2$ adsorption capacity at 800 Torr of 0.98 mmol of $CO_2$/mmol of MOF (1.23 mmol of $CO_2$ per g of MOF), which is approximately four times smaller than the overall capacity of **2** (Figure 3). The zero-coverage $Q_{st}$, 20 kJ/mol, was also significantly lower than the $Q_{st}$ of **2** (Figures S16–S19). Most notably, at 17 Torr, **2** adsorbed 0.99 mmol of $CO_2$ per mmol of MOF, which is approximately 300 times more $CO_2$ than **1** (0.0031 mmol of $CO_2$ per mmol of MOF) at the same pressure. The large uptake at low pressures demonstrates the potential utility of $CO_2$ insertion into the M–OH bond for $CO_2$ sorption applications.

Next, we investigated the ability of **1** and **2** to perform CA-like reactivity. The central function of CA is to rapidly interconvert $H_2O$ and $CO_2$ as well as bicarbonate and protons. We mimicked the interconversion *in vitro* by studying the exchange of $^{18}O$-labeled $H_2O$ with gaseous $CO_2$ and periodically sampling the headspace to monitor the distribution of $CO_2$ isotopologues by gas chromatography-mass spectroscopy. Notably, in the presence of **2**, the time to reach an equilibrium mixture of the three possible $CO_2$ isotopologues ($C^{16}O_2$, $C^{16,18}O_2$, and $C^{18}O_2$) was significantly reduced to 5 hr from 10 hr without **2** (Figures S28–S31). Consequently, there must be a rapid equilibrium for the Zn–OH + $CO_2$ ⇌ Zn–$OCO_2H$ and Zn–$OCO_2H$ + $H_2O$ ⇌ Zn–OH + $H_2CO_3$ reactions. It should be noted that **1** also decreased the time taken to reach an equilibrium mixture of the isotopologues but was not as effective as **2** because it reduced the equilibrium time to 7 hr. This could be attributed to partial hydrolysis of the Zn–Cl bond under the reaction conditions.

A second CA-like reaction often mimicked *in vitro* is the hydrolytic cleavage of 4-NPA. For instance, Jin and co-workers reported that the MOF CFA-1 ($Zn_5(OAc)_4$(bibta)$_3$, where bibta$^{2-}$ = 5,5′-bibenzo[d][1,2,3]triazole, **CFA-1**)[27] replicated the chemistry of CA through hydration of $CO_2$ and hydrolysis of 4-NPA.[28] Using similar reactivity conditions, we compared **1**, **2**, and **CFA-1** for their activity in the hydrolysis of 4-NPA (Figures S32–S34). The reactions were performed with ~2.5 mol % (10 mol % per Zn–X) MFU-4*l* (**1**) and MFU-4*l*-(OH) (**2**) in 50 mM HEPES buffer solution. They were sampled after 3, 6, 24, and 48 hr and were monitored by UV-vis spectroscopy for the formation of 4-nitrophenol (405 nm). A control reaction revealed small (1.7% ± 0.2%) conversion of 4-NPA after 24 hr in the absence of a MOF. Adding **1**, **2**, or **CFA-1** to the reaction mixture increased the conversion yield to 11% ± 2%, 15% ± 2%, and 14% ± 2%, respectively, at the 24 hr time point. In the conversion to mmol of product per mmol of Zn–X sites, this corresponds to low values of 1.2 ± 2, 1.8 ± 2, and 1.0 ± 1 for **1**, **2**, and **CFA-1**, respectively (Table S5). MFU-4*l*-(OH) **2** outperformed both **1** and **CFA-1**, most likely because **1** and **CFA-1** need to undergo ligand exchange to generate the Zn–OH active site. The low turnover number could be caused by pore blocking or slow diffusion through the micropores. Critically, this demonstrates that the $N_3$ZnOH coordination environment in **2** is a functional mimic of the CA reactivity.

In summary, we have demonstrated that the metal nodes of MFU-4*l* can be functionalized to create a high-fidelity biomimetic model of the CA active site. Reactions

performed by the enzymes, such as $CO_2$ insertion into the Zn–OH groups of the metal nodes and hydrolysis of 4-NPA, are mimicked in the MOF. These results demonstrate a rare example of functionalizing a MOF metal node to mimic the activity of an enzyme. The nascent field of biomimetic chemistry in MOFs holds potential for future understanding of enzyme chemistry and also the potential to perform enzyme-inspired reactions in stable frameworks. For instance, the insertion of $CO_2$ into a metal-hydroxide bond could lead to $CO_2$ separations with limited energy cost in regeneration, a concept we are currently exploring through implementing the chemistry of **2** in membrane composites for gas separations.

## SUPPLEMENTAL INFORMATION

Supplemental Information includes Supplemental Experimental Procedures, 36 figures, and 8 tables and can be found with this article online at https://doi.org/10.1016/j.chempr.2018.09.011.

## ACKNOWLEDGMENTS

This study was supported by the National Science Foundation (grant DMR-1452612) and used the Extreme Science and Engineering Discovery Environment, which is supported by National Science Foundation grant ACI-1548562.

## AUTHOR CONTRIBUTIONS

A.M.W. and M.D. conceptualized the experiments. A.M.W. synthesized materials and performed experiments. Z.W., G.Z., R.J.C., and J.T.M. collected and analyzed X-ray absorption spectroscopy data. R.W.D. and A.M.W. collected and analyzed X-ray photoelectron spectroscopy and energy-dispersive X-ray spectroscopy data. J.L.M. and C.H.H. performed computational studies. A.M.W. and M.D. wrote the original manuscript. All authors proofread, commented on, and approved the final manuscript for submission.

## DECLARATION OF INTERESTS

The authors declare no competing interests.

Received: June 25, 2018
Revised: July 16, 2018
Accepted: September 19, 2018
Published: October 4, 2018

## REFERENCES AND NOTES

1. Nath, I., Chakraborty, J., and Verpoort, F. (2016). Metal organic frameworks mimicking natural enzymes: a structural and functional analogy. Chem. Soc. Rev. *45*, 4127–4170.

2. Chen, Y., and Ma, S. (2016). Biomimetic catalysis of metal-organic frameworks. Dalton Trans. *45*, 9744–9753.

3. Chen, K., and Wu, C.D. (2018). Designed fabrication of biomimetic metal–organic frameworks for catalytic applications. Coord. Chem. Rev. Published online February 13, 2018. https://doi.org/10.1016/j.ccr.2018.01.016.

4. Zhao, M., Ou, S., and Wu, C.D. (2014). Porous metal-organic frameworks for heterogeneous biomimetic catalysis. Acc. Chem. Res. *47*, 1199–1207.

5. Gu, Z.Y., Park, J., Raiff, A., Wei, Z., and Zhou, H.C. (2014). Metal-organic frameworks as biomimetic catalysts. ChemCatChem *6*, 67–75.

6. Lykourinou, V., Chen, Y., Wang, X.S., Meng, L., Hoang, T., Ming, L.J., Musselman, R.L., and Ma, S. (2011). Immobilization of MP-11 into a mesoporous metal-organic framework, MP-11@mesoMOF: A new platform for enzymatic catalysis. J. Am. Chem. Soc. *133*, 10382–10385.

7. Li, P., Modica, J.A., Howarth, A.J., Vargas, L.E., Moghadam, P.Z., Snurr, R.Q., Mrksich, M., Hupp, J.T., and Farha, O.K. (2016). Toward design rules for enzyme immobilization in hierarchical mesoporous metal-organic frameworks. Chem *1*, 154–169.

8. Mehta, J., Bhardwaj, N., Bhardwaj, S.K., Kim, K.-H., and Deep, A. (2016). Recent advances in enzyme immobilization techniques: metal-organic frameworks as novel substrates. Coord. Chem. Rev. *322*, 30–40.

9. Li, P., Moon, S.Y., Guelta, M.A., Lin, L., Gómez-Gualdrón, D.A., Snurr, R.Q., Harvey, S.P., Hupp, J.T., and Farha, O.K. (2016). Nanosizing a metal-organic framework enzyme carrier for accelerating nerve agent hydrolysis. ACS Nano *10*, 9174–9182.

10. Liang, J.Y., and Lipscomb, W.N. (1990). Binding of substrate $CO_2$ to the active site of human carbonic anhydrase II: a molecular dynamics study. Proc. Natl. Acad. Sci. USA *87*, 3675–3679.

11. Parkin, G. (2004). Synthetic analogues relevant to the structure and function of zinc enzymes. Chem. Rev. *104*, 699–767.

12. Alsfasser, R., Vahrenkamp, H., Trofimenko, S., Looney, A., and Parkin, G. (1991). A mononuclear zinc hydroxide complex stabilized by a highly substituted tris(pyrazolyl) hydroborato ligand: analogies with the enzyme carbonic anhydrase. Inorg. Chem. *30*, 4098–4100.

13. Looney, A., Parkin, G., Alsfasser, R., Ruf, M., and Vahrenkamp, H. (1992). Zinc pyrazolylborate complexes relevant to the biological function of carbonic anhydrase. Angew. Chem. Int. Ed. *31*, 92–93.

14. Looney, A., Han, R., McNeill, K., and Parkin, G. (1993). Tris(pyrazolyl)hydroboratozinc hydroxide complexes as functional models for carbonic anhydrase: on the nature of the bicarbonate intermediate. J. Am. Chem. Soc. *115*, 4690–4697.

15. Biswas, S., Grzywa, M., Nayek, H.P., Dehnen, S., Senkovska, I., Kaskel, S., and Volkmer, D. (2009). A cubic coordination framework constructed from benzobistriazolate ligands and zinc ions having selective gas sorption properties. Dalton Trans. 6487–6495.

16. Denysenko, D., Werner, T., Grzywa, M., Puls, A., Hagen, V., Eickerling, G., Jelic, J., Reuter, K., and Volkmer, D. (2012). Reversible gas-phase redox processes catalyzed by co-exchanged MFU-4l(arge). Chem. Commun. (Camb.) *48*, 1236–1238.

17. Comito, R.J., Fritzsching, K.J., Sundell, B.J., Schmidt-Rohr, K., and Dincă, M. (2016). Single-site heterogeneous catalysts for olefin polymerization enabled by cation exchange in a metal-organic framework. J. Am. Chem. Soc. *138*, 10232–10237.

18. Denysenko, D., Grzywa, M., Jelic, J., Reuter, K., and Volkmer, D. (2014). Scorpionate-type coordination in MFU-4l metal-organic frameworks: small-molecule binding and activation upon the thermally activated formation of open metal sites. Angew. Chem. Int. Ed. *53*, 5832–5836.

19. Dubey, R.J., Comito, R.J., Wu, Z., Zhang, G., Rieth, A.J., Hendon, C.H., Miller, J.T., and Dincă, M. (2017). Highly stereoselective heterogeneous diene polymerization by Co-MFU-4l: a single-site catalyst prepared by cation exchange. J. Am. Chem. Soc. *139*, 12664–12669.

20. Wright, A.M., Rieth, A.J., Yang, S., Wang, E.N., and Dincă, M. (2018). Precise control of pore hydrophilicity enabled by post-synthetic cation exchange in metal-organic frameworks. Chem. Sci. (Camb.) *9*, 3856–3859.

21. Denysenko, D., Jelic, J., Reuter, K., and Volkmer, D. (2015). Postsynthetic metal and ligand exchange in MFU-4l: a screening approach toward functional metal-organic frameworks comprising single-site active centers. Chemistry *21*, 8188–8199.

22. Liao, P.-Q., Chen, H., Zhou, D.-D., Liu, S.-Y., He, C.-T., Rui, Z., Ji, H., Zhang, J.-P., and Chen, X.-M. (2015). Monodentate hydroxide as a super strong yet reversible active site for CO 2 capture from high-humidity flue gas. Energy Environ. Sci. *8*, 1011–1016.

23. Czepirski, L., and JagiełŁo, J. (1989). Virial-type thermal equation of gas-solid adsorption. Chem. Eng. Sci. *44*, 797–801.

24. Dincă, M., Dailly, A., Liu, Y., Brown, C.M., Neumann, D.A., and Long, J.R. (2006). Hydrogen storage in a microporous metal-organic framework with exposed Mn2+ coordination sites. J. Am. Chem. Soc. *128*, 16876–16883.

25. Sumida, K., Rogow, D.L., Mason, J.A., McDonald, T.M., Bloch, E.D., Herm, Z.R., Bae, T.H., and Long, J.R. (2012). Carbon dioxide capture in metal-organic frameworks. Chem. Rev. *112*, 724–781.

26. Bräuer, M., Pérez-Lustres, J.L., Weston, J., and Anders, E. (2002). Quantitative reactivity model for the hydration of carbon dioxide by biomimetic zinc complexes. Inorg. Chem. *41*, 1454–1463.

27. Schmieder, P., Denysenko, D., Grzywa, M., Baumgärtner, B., Senkovska, I., Kaskel, S., Sastre, G., van Wüllen, L., and Volkmer, D. (2013). CFA-1: the first chiral metal-organic framework containing Kuratowski-type secondary building units. Dalton Trans. *42*, 10786–10797.

28. Jin, C., Zhang, S., Zhang, Z., and Chen, Y. (2018). Mimic carbonic anhydrase using metal-organic frameworks for $CO_2$ capture and conversion. Inorg. Chem. *57*, 2169–2174.